

Detection of 2460 SB2 candidates in the LAMOST-MRS, using projected rotational velocities and a binary spectral model.

Mikhail Kovalev^{1,2,3,4★}, Xuefei Chen^{1,2,5}, Zhanwen Han^{1,2,5}

¹Yunnan Observatories, China Academy of Sciences, Kunming 650216, China

²Key Laboratory for the Structure and Evolution of Celestial Objects, Chinese Academy of Sciences, Kunming 650011, China

³Sternberg Astronomical Institute, Leninskie Gory, Moscow 119992, Russia

⁴Max Planck Institute for Astronomy, D-69117 Heidelberg, Germany

⁵Center for Astronomical Mega-Science, Chinese Academy of Sciences, 20A Datun Road, Chaoyang District, Beijing 100012, China

Accepted 31-08-2022. Received 24-08-2022; in original form 15-07-2022

ABSTRACT

We present a new method for the detection of double-lined spectroscopic binaries (SB2) using $V \sin i$ values from spectral fits. The method is tested on synthetic and real spectra from LAMOST-MRS. It can reliably detect SB2 candidates for double-lined binaries with $V \sin i_1 + V \sin i_2 < 300 \text{ km s}^{-1}$ if the radial velocity separation is large enough. Using this method, we detect 2460 SB2 candidates, 1410 of which are new discoveries. We confirm the correlation between the radial velocity separation estimated by the binary model and $V \sin i_0$ estimated by the single star model using the selected sample. Additionally, our method finds one new SB2 candidate in open cluster M 11.

Key words: binaries : spectroscopic – techniques : spectroscopic – stars individual: J115307.93+353528.2, J005425.62+081141.3, J064726.39+223431.7, J065032.45+231030.2, J055923.95+303104.02, J065001.65+222127.7, J053818.60-091754.4.

1 INTRODUCTION

Modern spectroscopic surveys provide a huge amount of stellar spectra. Traditionally, the main analysis of survey data is focused on single stars, while spectroscopic binaries (SBn, where n is a number of spectral components) should be removed and analysed separately. SB2s with non-zero radial velocity separation ($|\Delta RV| = |RV_1 - RV_2|$) of spectral components are usually detected by analysis of multiple peaks of the cross-correlation functions (CCF) (Merle et al. 2017; Li et al. 2021; Kounkel et al. 2021), although it is possible to detect an SB2 with $|\Delta RV| = 0$ using composite spectroscopic model (El-Badry et al. 2018; Kovalev & Straumit 2022) if spectral components are significantly different. Machine learning techniques are also used to find SB2s (Traven et al. 2020; Zhang et al. 2022).

Kovalev & Straumit (2022) selected SB2 candidates in open cluster M 11 by visual inspection of the spectra, which showed a significant improvement of the fit, when using the composite spectral model. They found a clear correlation between the $|\Delta RV|$ estimated by the binary model and the value of the projected rotational velocity $V \sin i_0$, derived from the single-star model for SB2 systems, and proposed to use this correlation for SB2 identification. In this work we develop this idea further as a new method for SB2 detection, thereby finding one new SB2 candidate in the previous M 11

data set and successfully apply it to detect 2460 SB2 candidates in the LAMOST (Large Sky Area Multi-Object fiber Spectroscopic Telescope) Medium Resolution Survey (MRS) (Liu et al. 2020).

The paper is organised as follows: in Sections 2 and 3, we describe the observations and methods. Section 4 presents our results. In Section 5 we discuss the results. In Section 6 we summarise the paper and draw conclusions.

2 OBSERVATIONS

LAMOST is a 4-meter quasi-meridian reflective Schmidt telescope with 4000 fibers installed on its 5° FoV focal plane. These configurations allow it to observe spectra for at most 4000 celestial objects simultaneously (Cui et al. (2012); Zhao et al. (2012)). For the analysis in this paper, we downloaded all available time-domain spectra from www.lamost.org. We use the spectra taken at a resolving power of $R = \lambda/\Delta\lambda \sim 7500$. Each spectrum is divided on two arms: blue from 4950 Å to 5350 Å and red from 6300 Å to 6800 Å. We convert the heliocentric wavelength scale in the observed spectra from vacuum to air using PyAstronomy (Czesla et al. 2019). Observations are carried out in MJD=58407.6-59567.8 days, spanning an interval of 1160 days. We selected only spectra stacked for whole

★ E-mail: mikhail.kovalev@ynao.ac.cn

night¹ and apply a cut on the signal-to-noise (S/N). In total we have 592 060 spectra from 138 114 targets, where the $S/N \geq 25 \text{ pix}^{-1}$ in any of spectral arms. The majority of the spectra (one half) sample the S/N in the range of 40–250 pix^{-1} . The number of exposures varies from 1 to 27 per target, as noisy exposures were not selected for many targets.

For M 11 stars we use 265 infrared spectra from Gaia-ESO survey (Gilmore et al. 2012). They were observed with the GIRAFFE (Pasquini et al. 2002) instrument on the VLT (Very Large Telescope) of the European Southern Observatory (ESO) using the HR21 setup ($\lambda = 8475 - 8980 \text{ \AA}$, $R = 16\,200$) and have S/N in the range from 30 to 120 pix^{-1} . For a detailed description of the M 11 dataset we refer the reader to Kovalev & Straumit (2022).

3 METHODS

3.1 Spectroscopic analysis

The results for M 11 stars were taken from the previous work Kovalev & Straumit (2022).

We use the same spectroscopic models and method as Kovalev et al. (2022) to analyse individual LAMOST-MRS spectra, see brief description below. The normalised binary model spectrum is generated as a sum of the two Doppler-shifted normalised single-star spectral models $f_{\lambda,i}$ ², scaled according to the difference in luminosity, which is a function of the T_{eff} and stellar size. We assume both components to be spherical and use the following equation:

$$f_{\lambda,\text{binary}} = \frac{f_{\lambda,2} + k_{\lambda} f_{\lambda,1}}{1 + k_{\lambda}}, \quad k_{\lambda} = \frac{B_{\lambda}(T_{\text{eff},1}) M_1}{B_{\lambda}(T_{\text{eff},2}) M_2} 10^{\log(g)_2 - \log(g)_1} \quad (1)$$

where k_{λ} is the luminosity ratio per wavelength unit, B_{λ} is the black-body radiation (Planck function), T_{eff} is the effective temperature, $\log(g)$ is the surface gravity and M is the mass. Throughout the paper we always assume the primary star to be brighter and define mass ratio as $q = M_1/M_2$, which is inverted in comparison with traditional definition $Q = 1/q$.

The binary model spectrum is later multiplied by the normalisation function, which is a linear combination of the first four Chebyshev polynomials (similar to Kovalev et al. 2019), defined separately for the blue and red arms of the spectrum. The resulting spectrum is compared with the observed one using `scipy.optimize.curve_fit` function, which provides the optimal spectral parameters and radial velocities (RV) for each component plus the mass ratio $q = M_1/M_2$ and two sets of four coefficients of the Chebyshev polynomials. We keep the metallicity equal for both components. In total we have 18 free parameters for a binary fit. We estimate the goodness of the fit parameter by reduced χ^2 .

Additionally, every spectrum is analysed by a single star model, which is identical to a binary model when both components have all equal parameters, so we fit only for 13 free parameters. Using this single star solution³ we compute the difference in reduced χ^2 between two solutions and the improvement factor (f_{imp}), computed

using Equation 2 similar to El-Badry et al. (2018). This improvement factor estimates the absolute value difference between two fits and weights it by the difference between the two solutions.

$$f_{\text{imp}} = \frac{\sum \left[\left(|f_{\lambda,\text{single}} - f_{\lambda}| - |f_{\lambda,\text{binary}} - f_{\lambda}| \right) / \sigma_{\lambda} \right]}{\sum \left[|f_{\lambda,\text{single}} - f_{\lambda,\text{binary}}| / \sigma_{\lambda} \right]}, \quad (2)$$

where f_{λ} and σ_{λ} are the observed flux and corresponding uncertainty, $f_{\lambda,\text{single}}$ and $f_{\lambda,\text{binary}}$ are the best-fit single-star and binary model spectra, and the sum is over all wavelength pixels.

The current paper focuses on SB2 identification of a single epoch spectrum, and we will present the results of the simultaneous analysis of the multiple spectra in our future paper (Kovalev et al. in prep).

3.2 Selection of SB2 candidates using rotational velocities

The logic of the selection is quite simple: we need to separate single stars from all binary solutions. If we try to fit the double-lined spectrum with $|\Delta \text{RV}| > 0$ using a single star model there are three possible outcomes:

- (i) none of the spectral components are well constrained, but $V \sin i_0$ proportional to $|\Delta \text{RV}|$ is large enough that broadened model covers both of them;
- (ii) only one spectral component (usually the primary) is well fitted, while the other is completely ignored by the spectral model;
- (iii) the spectrum is poorly fitted as the synthetic model is unable to reproduce a real spectrum due to missing physics (usually emission lines, molecular bands etc.) or data processing artifacts.

For all these cases binary model fits the spectrum much better and f_{imp} is big. However only case (i) is useful to select SB2s. Even small $|\Delta \text{RV}|$, which is insufficient to split spectral lines due to finite spectrograph's resolution, will cause change to the spectral lines: they will become broader and the fitted value of $V \sin i_0$ will increase in comparison with the value from the spectrum of that binary taken when $|\Delta \text{RV}| = 0$. Case (ii) can be excluded by requiring RV_1 to differ from RV_0 , as such a case is useless for SB2 identification. However, it can be used, when several observations are available for a given target. Multiple epochs allow us to find an SB2 candidate by $V \sin i_0$ variation, which it is proportional to $|\Delta \text{RV}|$, although such a variation can be caused by a real change of $V \sin i$.

Now we need to separate out the single stars. When a single star spectrum with $V \sin i_0$ is fitted by a binary model there are three possible outcomes:

- (i) the spectrum is well fitted by twin binary model, consisting of two components similar to the real star with small $|\Delta \text{RV}| \sim 0$, therefore $V \sin i_{1,2} \sim V \sin i_0$ and $V \sin i_1 + V \sin i_2 \sim 2V \sin i_0$;
- (ii) the spectrum is well fitted by the primary component, which is almost identical to the real star ($V \sin i_1 \sim V \sin i_0$), and a small or negligible contribution from the secondary component, which can have any value $V \sin i_2$, although usually it is quite large, so the secondary spectrum looks completely “flat”;
- (iii) the spectrum is poorly fitted as the synthetic model is unable to reproduce the real spectrum. In this case, the binary model is desperately trying to compensate for the missing spectral information by combining two spectral components, usually with significant improvement relative to best single star model.

For cases (i) and (ii) f_{imp} is usually small, but for case (iii) it can be quite large. Thus we can select SB2 candidates with $|\Delta \text{RV}| > 0$ by

¹ Each exposure contains a sequence of the several short 20 min individual exposures, which were stacked to increase S/N, see Appendix B1.1 with example of non-stacked spectra.

² they are designed as a good representation of the LAMOST-MRS spectra, see Appendix A for details

³ throughout paper it has subscript “0” or “single”

selecting the spectra with $V \sin i_1 + V \sin i_2 + V \sin i_{\min} < V \sin i_0$ and $RV_1 \neq RV_0$, while “bad fits” from case (iii) can be excluded using a cut on f_{imp} . $V \sin i_{\min}$ takes into account the possible uncertainties in the $V \sin i$ measurements. However we should note that these criteria will not select spectra of fast rotators, as in this case $V \sin i_1 + V \sin i_2 > V \sin i_0$ for small $|\Delta RV| > 0$. They can be selected only for a significant $|\Delta RV|$. One can find various fit examples in Appendix B.

3.2.1 Test on synthetic SB2s

Kovalev & Straumit (2022) presented spectral simulations for open cluster M 11 with 1480 SB2s and 480 single stars, where 480 SB2s are twin binaries, with all identical parameters for components except for RV. Each star had only one spectrum. We take these results and plot $V \sin i_1 + V \sin i_2$ versus $V \sin i_0$ in the top panel of Fig. 1. Solid lines show the functions $V \sin i_1 + V \sin i_2 = V \sin i_0$ (blue) and $V \sin i_1 + V \sin i_2 = 2V \sin i_0$ (red). It is clearly seen that the single star subset mostly follows the red line and there are no single stars below the blue line. Mock binary stars populate the entire parameter space between zero and the dashed line $V \sin i_1 + V \sin i_2 = 330 + V \sin i_0$. We select only datapoints $V \sin i_{\min} = 5 \text{ km s}^{-1}$ below the blue line with $f_{\text{imp}} > 0.1$ and $|RV_1 - RV_0| > 5 \text{ km s}^{-1}$ as SB2 candidates, to exclude all spectra from the single-star subset. In total we have 76 spectra, 59 of them are twin binaries, therefore success rate (SR) of our selection method is $SR = 76/1480 = 0.05$ for all SB2s and $SR_{\text{twins}} = 59/480 = 0.125$ for twins. The success rate is small, because this simulated dataset mostly contains fast rotators with small $|\Delta RV|$.

Therefore for the time-domain LAMOST-MRS we create a new simulated set with larger $|\Delta RV|$ and several spectra per star, using binary spectral model from Section 3.1. We generate 10000 mock binaries using uniformly distributed mass-ratios $Q = M_2/M_1 = U(0.01, 1.0)$, T_{eff} from 4600 to 8800 K, $\log(g)$ from 2.6 to 4.8 (cgs), $V \sin i = U(1, 200) \text{ km s}^{-1}$ for both components and $[\text{Fe}/\text{H}]_1 = [\text{Fe}/\text{H}]_2 = U(-0.36, 0.36) \text{ dex}$. For each star, we create five mock binary spectra using radial velocities computed for circular orbits with the random semiamplitudes $K_2 = U(0, 300)$, $K_1 = QK_2 \text{ km s}^{-1}$ at randomly chosen phases. These models are degraded by Gaussian noise according to $S/N = 50$, 100 pix^{-1} for the blue and red spectral arms respectively. Such models serve as a good representation of the real LAMOST-MRS observations. We compute the secondary contribution to the total light at $\lambda = 5000 \text{ \AA}$ as $\text{frac} = 1/(1 + k_{5000})$ and selected 1411 stars with $\text{frac} < 0.01$ (below noise level) as a subset of the single stars with 7044 spectra.

We perform exactly the same analysis as for the observations on this simulated dataset (see Section 3.1). We checked how well the parameters can be recovered by calculating the average and standard deviation of the residuals. For the single stars we have $\Delta RV = 0.03 \pm 0.32 \text{ km s}^{-1}$, $\Delta T_{\text{eff}0} = 34 \pm 64 \text{ K}$, $\Delta \log(g)_0 = 0.05 \pm 0.08 \text{ cgs units}$, $\Delta V \sin i_0 = -1 \pm 2 \text{ km s}^{-1}$ and $\Delta[\text{Fe}/\text{H}]_0 = 0.02 \pm 0.04 \text{ dex}$. For the primary components we have $\Delta RV_1 = -0.02 \pm 12.63 \text{ km s}^{-1}$, $\Delta T_{\text{eff}1} = 11 \pm 192 \text{ K}$, $\Delta \log(g)_1 = 0.05 \pm 0.14 \text{ cgs units}$, $\Delta V \sin i_1 = 0 \pm 13 \text{ km s}^{-1}$. For the secondary components we have $\Delta RV_2 = 1.35 \pm 72.58 \text{ km s}^{-1}$, $\Delta T_{\text{eff}2} = 157 \pm 891 \text{ K}$, $\Delta \log(g)_2 = 0.29 \pm 0.55 \text{ cgs units}$, $\Delta V \sin i_2 = -23 \pm 60 \text{ km s}^{-1}$. Metallicity has $\Delta[\text{Fe}/\text{H}]_{1,2} = 0.01 \pm 0.04 \text{ dex}$. The mass ratio is recovered poorly $\Delta Q = -0.05 \pm 0.33$, and thus is mostly unreliable. It is clear that the parameters of the secondary components are poorly recovered compared to the primary components, especially $\log(g)_2$. However accurate spectral parameters are not critical for

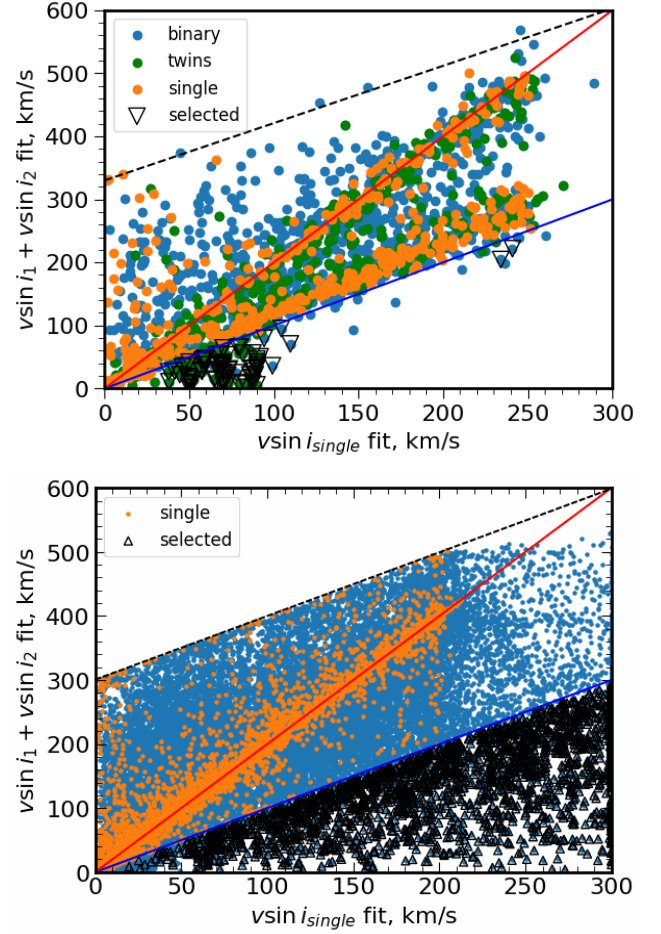


Figure 1. Example of the selection using $V \sin i$ for simulated datasets of M 11 (top) and LAMOST-MRS (bottom). Solid lines show the functions $V \sin i_1 + V \sin i_2 = V \sin i_0$ (blue) and $V \sin i_1 + V \sin i_2 = 2V \sin i_0$ (red).

the purpose of SB2 identification, as binary model serves as a “flexible template”. The simultaneous analysis of multiple epochs have a much better impact on a parameter’s recovery (Kovalev et al. 2022).

We show the selection of SB2 candidates using $V \sin i$ on bottom panel of Fig. 1. Solid lines show the functions $V \sin i_1 + V \sin i_2 = V \sin i_0$ (blue) and $V \sin i_1 + V \sin i_2 = 2V \sin i_0$ (red). It is clearly seen that the single star subset mostly follows the red line and no single stars are seen below the blue line. Mock binary stars populate all parameter space between zero and dashed line $V \sin i_1 + V \sin i_2 = 300 + V \sin i_0$. We select all datapoints $V \sin i_{\min} = 5 \text{ km s}^{-1}$ below the blue line with $f_{\text{imp}} > 0.1$ and $|RV_1 - RV_0| > 10 \text{ km s}^{-1}$ as SB2 candidates. In total we have 2127 spectra of 1112 stars (zero from the single star subset), where all five spectra are selected for 22, four for 74, three for 189, two for 327 and only one for 500 mock binaries respectively. Therefore the success rate of our selection method is around $SR = 1112/(10000 - 1411) = 0.129$.

In our selection we prioritize purity over completeness, thus SR is relatively small. One can use less strict quality cuts on $V \sin i_{\min}$, f_{imp} and $|RV_1 - RV_0|_{\min}$, however it can produce many false-positive detections. If multiple epochs are available one can find more SB2 candidates using $V \sin i_0$ variation with time. We

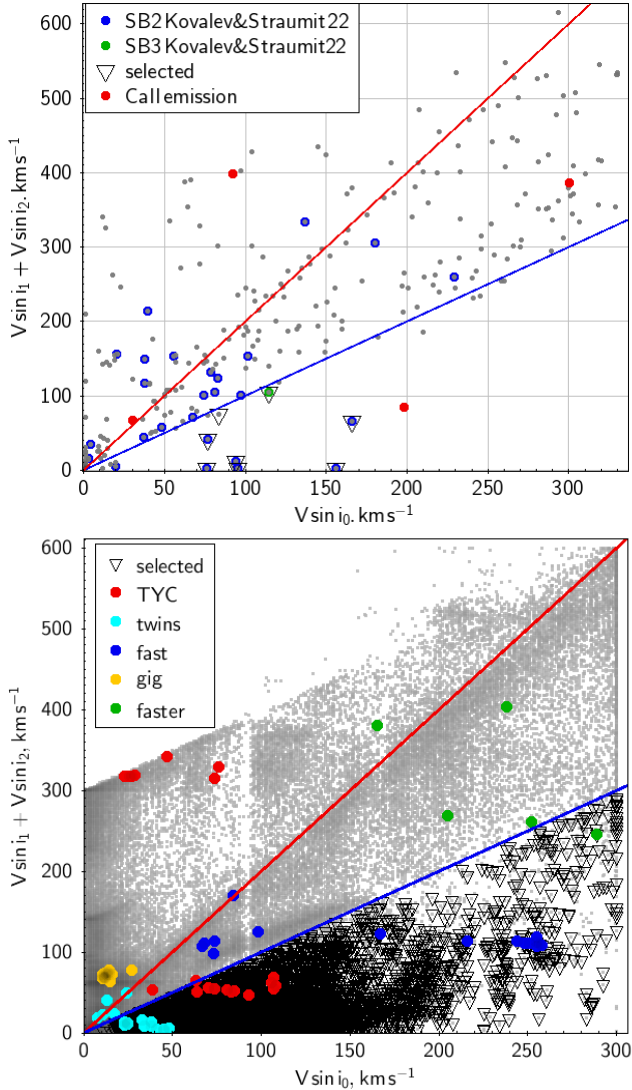


Figure 2. Example of the SB2 selection using $V \sin i$ for observed datasets of M 11 (top panel) and LAMOST-MRS (bottom panel). Solid lines show the functions $V \sin i_1 + V \sin i_2 = V \sin i_0$ (blue) and $V \sin i_1 + V \sin i_2 = 2V \sin i_0$ (red). Selected stars are shown with black open triangles. Several confirmed SB2s are highlighted.

plan to implement this in improved selection method in our future paper (Kovalev et al. in prep.).

4 RESULTS

4.1 Application to binaries from M 11

We use our criteria to explore the data from Kovalev & Straumit (2022). We show $V \sin i$ plot in the top panel of Fig. 2. Four spectra with strong emission at Ca II lines are shown as red circles, they are poorly fitted based on visual inspection. We find that the new criteria select eight SB2 candidates out of 265 spectra, shown as black open triangles. All SB2s and SB3 candidates from Kovalev & Straumit (2022) are shown as blue and green circles, where seven are selected, thus we find one new SB2 candidate. We discuss them in Appendix D.

Table 1. Quality cuts

Filtering bad fits - any of the following cuts
$\chi^2_{\text{single}} > 120$
$ \Delta RV > 320 \text{ km s}^{-1}$
$ RV_0 > 400 \text{ km s}^{-1}$
$ \log q > 0.95$
$k_{5000}/(1 + k_{5000}) > 0.95$
$[[\text{Fe}/\text{H}]_0] > 0.85$ and $V \sin i_0 > 299 \text{ km s}^{-1}$
$ \log(g)_0 - 3 > 1.98$ and $V \sin i_0 > 299 \text{ km s}^{-1}$
$ \log(g)_0 - 3 > 1.98$ and $T_{\text{eff}0} > 8780 \text{ K}$
$ \log(g)_1 - 3 > 1.98$ and $T_{\text{eff}1} > 8780 \text{ K}$
Bad λ calibration in 213 spectra

4.2 LAMOST-MRS

4.2.1 Quality cuts

We carefully check the quality of the spectral fits through visual inspection of the plots. Our LAMOST-MRS dataset contains spectra from various targets and some of them can be poorly fitted by our spectral model (red super giants, very hot stars, see Fig. B7). Therefore we introduce several quality cuts on the fitted parameters, see Table 1. They exclude 192 533 spectra (33 per cent) from the data set. Additionally we find 213 spectra, where wavelength scale is clearly shifted between the blue and left arms, see Appendix B3.

4.2.2 Selected SB2 candidates

We show the selection of SB2 candidates using $V \sin i$ on the bottom panel of Fig. 2. It is clearly seen that not selected stars slightly follow red and blue lines. We have a large overdensity at $V \sin i_0 = 1 \text{ km s}^{-1}$ and there is a clear gap at $V \sin i_0 \sim 90 \text{ km s}^{-1}$. We currently do not have a clear explanation for this gap, perhaps caused by a systematic problem in the fitting mechanism, since there is weak evidence of a similar gap for the simulated LAMOST-MRS dataset shown in Fig. 1. Selected SB2s candidates are shown by open black triangles, with the majority having $V \sin i_0$ in the interval from 20 to 150 km s^{-1} . In total we have 6160 spectra from 2460 stars, listed in Table C1. For several confirmed SB2s we highlight all available spectra as filled circles. It is clearly seen that many such spectra follow horizontal lines of nearly constant $V \sin i_1 + V \sin i_2$. For example the Algol-like system TYC 2990-127-1 ($q = 4.75$) from Kovalev et al. (2022) is labeled as “TYC” (red circles). Many spectra are selected, although several spectra taken near conjunction phase are fitted with very big $V \sin i_2$. Twin binary (cyan circles) with unresolved double-lined spectrum is selected many times, but some spectra with $|\Delta RV| \sim 0$ follow the red line. Two systems of fast rotators, labeled as “fast” and “faster” are shown as blue and green circles. For “fast” fits of several spectra, where single star model was ignoring secondary component (case (ii)), are not selected. In the “faster” only one spectrum is selected. Fits for these three SB2s are shown in Fig. B1. We also show as gold circles an interesting SB2 system with very different spectral components ($\Delta T_{\text{eff}} > 3000 \text{ K}$) labeled as “gig”. None of its spectra are selected due to small $|\Delta RV|$ and fast rotation of the hotter component, see Fig. B5. This star can be selected based on big $f_{\text{imp}} > 0.3$. We will present a detailed study of it in our future paper.

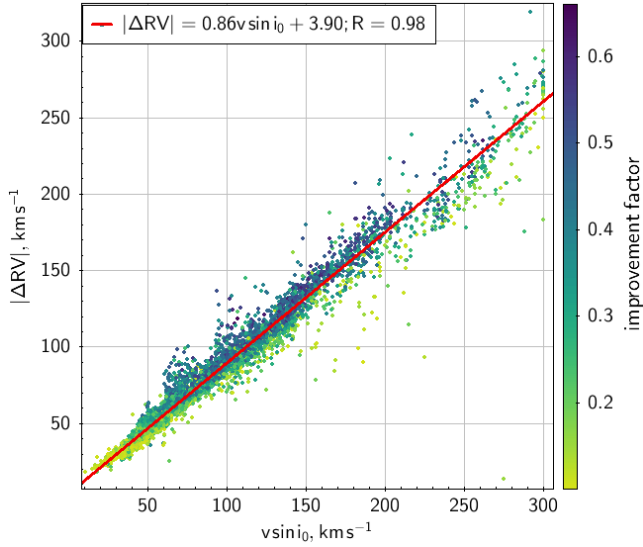


Figure 3. Correlation between $|\Delta RV|$ and $V \sin i_0$ for selected SB2s.

5 DISCUSSION

We plot $|\Delta RV|$ and $V \sin i_0$ for all selected spectra and confirm the correlation between these parameters. We fit a straight line through the data points using f_{imp} as a weight and find:

$$|\Delta RV| = 0.86 V \sin i_0 + 3.90, R = 0.98, \quad (3)$$

where R is a Pearson's product moment correlation coefficient. Since we have $V \sin i_{\text{min}} = 5 \text{ km s}^{-1}$ as our selection criteria, in theory we can select SB2s with $|\Delta RV| = 8.2 \text{ km s}^{-1}$ based on this fit. The minimal $|\Delta RV| \sim 20 \text{ km s}^{-1}$, among selected SB2s, which is much smaller than $|\Delta RV| = 50 \text{ km s}^{-1}$, required by CCF based methods developed for LAMOST-MRS spectra (Li et al. 2021), therefore our method should be able to find more SB2 candidates. However, many SB2s are still not detected, especially when the single star model fits only one component (case (ii)) or the spectrum was observed at moment of small $|\Delta RV|$, see Appendix B1.2.

We check how usage of stacked spectra can alter the fitting results in Appendix B1.1. We find that for close SB2 with period $P < 2$ days, stacking of 5 consecutive 20 min exposures leads to slight increase of $V \sin i_{1,2}$ by 3 – 5 km s^{-1} in stacked spectrum, due to blurring. Therefore short epochs are more useful for close SB2s.

5.1 Comparison with other SB2 catalogues

We make cross matches with several available SB2 catalogues. We find 17 matches with SIMBAD database (Wenger et al. 2000), labeled as SB*, two matches with SB9 (Pourbaix et al. 2004), 56 matches with Traven et al. (2020), and 108 matches with Kounkel et al. (2021) catalogues. Cross matching with El-Badry et al. (2018) we find 10 stars listed in their SB2 table. Surprisingly, we find one match with their single star table and one match with the SB1 table. We check these matches and confirm that they are SB2 candidates, see Fig. B3. We find no matches with either the SB3 table or the SB2 table with unseen third component. Among LAMOST-MRS based papers we find 535 SB2 matches and 24 SB3 matches with Li et al. (2021), 173 matches with Wang et al. (2021) and 440 matches with

Zhang et al. (2022)⁴. We find 122 matches with recent Gaia DR3 non-single stars orbits catalogue (Gaia Collaboration et al. 2022a).

In total our catalogue includes 1050 known and 1410 new SB2 candidates. Also some of them are possibly SB3s, see Fig. B2. However we should note that some SB2 candidates can be chance alignments due to relatively large fiber diameter of the spectrograph ($3''$). Our sample is limited to time-domain spectra with $S/N > 25$, therefore the number of matches with other LAMOST-MRS based studies is not very high. We plan to extend it to non time-domain spectra in our future paper.

5.2 Gaia DR3 data for LAMOST-MRS dataset

We check the recent Gaia DR3 (Gaia Collaboration et al. 2016, 2022b) and plot the Hertzsprung-Russell diagram for all matches with positive parallax in top panel of Fig. 4. Selected SB2 candidates are shown with black open triangles. Some of them are located at the main sequence of binaries with similar luminosity which is ~ 0.75 mag higher than main sequence. Gaia DR3 provides parameter v_{broad} as a measure of rotational broadening for a single stars, based on Gaia RVS spectra (Frémat et al. 2022). We use it instead of $V \sin i_0$ and reproduce bottom panel of Fig. 2 in the bottom panel of Fig. 4. Again is clearly seen that not selected stars slightly follow the red and blue lines. We have an overdensity at $v_{\text{broad}} < 10 \text{ km s}^{-1}$, and we have many hot stars in the region higher than the black dashed line $V \sin i_1 + V \sin i_2 = v_{\text{broad}} + 300$. In Fig. 2 it was empty, because our fitting algorithm is unable fit $T_{\text{eff}} > 8800 \text{ K}$, so it tries to increase $V \sin i_0$ in order to compensate for changes in the spectra. We apply the same selection as before using v_{broad} instead of $V \sin i_0$ and find 1380 spectra of 491 stars, where 436 of them were previously selected using $V \sin i_0$. We show them as green circles. The remaining 55 stars were probably observed by LAMOST-MRS at moments with $|\Delta RV| \sim 0 \text{ km s}^{-1}$. Unfortunately we can't check this hypothesis, because epoch's RVS spectra and RV measurements aren't included in Gaia DR3. However this confirms that Frémat et al. (2022) were unable to completely filter out SB2s from their catalogue.

6 CONCLUSIONS

We developed a new method for SB2 detection in spectral surveys. It is based on the simple fact that single star model will fit the SB2 spectrum with large rotational broadening $V \sin i_0$, proportional to the $|\Delta RV|$. This method found eight (one new) SB2 candidates in the M 11 cluster and 2460 (1410 new) SB2 candidates in the LAMOST-MRS. We will present a detailed study of the spectral parameters and orbits (similar to one in Kovalev et al. (2022)) of LAMOST-MRS SB2 candidates in our future paper. We hope that our method will be useful in SB2 detection in large-scale spectroscopic surveys, e.g. Gaia RVS (Cropper et al. 2018).

ACKNOWLEDGEMENTS

We are grateful to the anonymous referee for a constructive report. We thank Hans Bähr for his careful proof-reading of the manuscript. MK is grateful to his parents, Yuri Kovalev and Yulia Kovaleva, for their full support in making this research possible. MK thanks Maria Kovaleva for valuable discussions. This

⁴ among their final sample of 2198 SB2 candidates

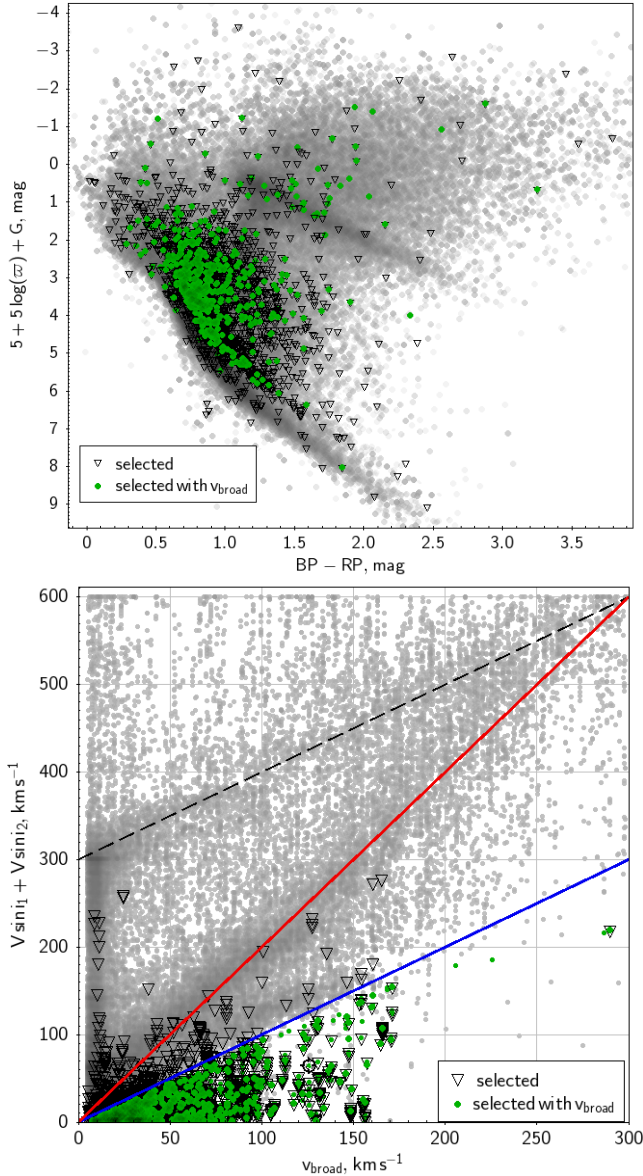


Figure 4. Gaia DR3 Hertzsprung-Russell diagram for observed LAMOST-MRS dataset (top panel) and $V \sin i_1 + V \sin i_2$ versus v_{broad} (bottom panel). SB2 candidates selected in Fig. 2 are shown with open black triangles, SB2 candidates selected using v_{broad} are shown with green circles.

work is supported by National Key R&D Program of China (Grant No. 2021YFA1600401/3), and by the Natural Science Foundation of China (Nos. 12090040/3, 12125303, 11733008). Guoshoujing Telescope (the Large Sky Area Multi-Object Fiber Spectroscopic Telescope LAMOST) is a National Major Scientific Project built by the Chinese Academy of Sciences. Funding for the project has been provided by the National Development and Reform Commission. LAMOST is operated and managed by the National Astronomical Observatories, Chinese Academy of Sciences. The authors gratefully acknowledge the “PHOENIX Supercomputing Platform” jointly operated by the Binary Population Synthesis Group and the Stellar Astrophysics Group at Yunnan Observatories, Chinese Academy of Sciences. This work has made use of data from the European Space Agency (ESA) mission

Gaia (<https://www.cosmos.esa.int/gaia>), processed by the *Gaia* Data Processing and Analysis Consortium (DPAC, <https://www.cosmos.esa.int/web/gaia/dpac/consortium>). Funding for the DPAC has been provided by national institutions, in particular the institutions participating in the *Gaia* Multilateral Agreement. Based on data products from observations made with ESO Telescopes at the La Silla Paranal Observatory under run IDs 188.B-3002 and 193.B-0936. This research has made use of NASA’s Astrophysics Data System, the SIMBAD data base, and the VizieR catalogue access tool, operated at CDS, Strasbourg, France. It also made use of TOPCAT, an interactive graphical viewer and editor for tabular data (Taylor 2005).

DATA AVAILABILITY

The data underlying this article will be shared on reasonable request to the corresponding author. LAMOST-MRS spectra are downloaded from www.lamost.org. The M 11 data are based on public spectra downloaded from http://archive.eso.org/wdb/wdb/adp/phase3_spectral/form?collection_name=GAIAESO

REFERENCES

- Cropper M., et al., 2018, *A&A*, **616**, A5
 Cui X.-Q., et al., 2012, *Research in Astronomy and Astrophysics*, **12**, 1197
 Czesla S., Schröter S., Schneider C. P., Huber K. F., Pfeifer F., Andreasen D. T., Zechmeister M., 2019, PyA: Python astronomy-related packages (ascl:1906.010)
 El-Badry K., et al., 2018, *MNRAS*, **476**, 528
 Frémat Y., et al., 2022, arXiv e-prints, p. arXiv:2206.10986
 Gaia Collaboration et al., 2016, *A&A*, **595**, A1
 Gaia Collaboration et al., 2021, *A&A*, **649**, A1
 Gaia Collaboration et al., 2022a, arXiv e-prints, p. arXiv:2206.05595
 Gaia Collaboration et al., 2022b, arXiv e-prints, p. arXiv:2208.00211
 Gilmore G., et al., 2012, *The Messenger*, **147**, 25
 Kounkel M., et al., 2021, arXiv e-prints, p. arXiv:2107.10860
 Kovalev M., 2019, PhD thesis, IMPRS-HD, doi:10.11588/heidok.00027411, https://www.imprs-hd.mpg.de/408002/thesis_Kovalev.pdf
 Kovalev M., Straumit I., 2022, *MNRAS*, **510**, 1515
 Kovalev M., Bergemann M., Ting Y.-S., Rix H.-W., 2019, *A&A*, **628**, A54
 Kovalev M., Li Z., Zhang X., Li J., Chen X., Han Z., 2022, *MNRAS*, **513**, 4295
 Li C.-q., Shi J.-r., Yan H.-l., Fu J.-N., Li J.-d., Hou Y.-H., 2021, *ApJS*, **256**, 31
 Liu C., et al., 2020, arXiv e-prints, p. arXiv:2005.07210
 Merle T., et al., 2017, *A&A*, **608**, A95
 Pasquini L., et al., 2002, *The Messenger*, **110**, 1
 Pourbaix D., et al., 2004, *A&A*, **424**, 727
 Taylor M. B., 2005, in Shopbell P., Britton M., Ebert R., eds, *Astronomical Society of the Pacific Conference Series Vol. 347, Astronomical Data Analysis Software and Systems XIV*. p. 29
 Ting Y.-S., Conroy C., Rix H.-W., Cargile P., 2019, *ApJ*, **879**, 69
 Traven G., et al., 2020, *A&A*, **638**, A145
 Wang S., et al., 2021, arXiv e-prints, p. arXiv:2109.03149
 Wenger M., et al., 2000, *A&AS*, **143**, 9
 Zhang B., et al., 2022, *ApJS*, **258**, 26
 Zhao G., Zhao Y.-H., Chu Y.-Q., Jing Y.-P., Deng L.-C., 2012, *Research in Astronomy and Astrophysics*, **12**, 723

APPENDIX A: SPECTRAL MODEL FOR LAMOST-MRS

The grid of synthetic spectra (6200 in total) is generated using the NLTE MPIA online-interface <https://nlte.mpia.de> (see Chap-

ter 4 in Kovalev 2019) on wavelength intervals 4870:5430 Å for the blue arm and 6200:6900 Å for the red arm with spectral resolution $R = 7500$. We use a NLTE (non-local thermodynamic equilibrium) spectral synthesis for H, Mg I, Si I, Ca I, Ti I, Fe I and Fe II lines (see Chapter 4 in Kovalev 2019, for references). The spectral parameters are randomly selected in a range of $T_{\text{eff}}=4600, 8800$ K, $\log(g)=1.0, 4.99$ (cgs units), $V \sin i=1, 300 \text{ km s}^{-1}$ and $[\text{Fe}/\text{H}]^5=-0.9, +0.9$ dex, microturbulence is fixed to $V_{\text{mic}} = 2 \text{ km s}^{-1}$. The grid is randomly split on training (70%) and cross-validation (30%) sets of spectra, which are used to train *The Payne* spectral model (Ting et al. 2019). We use output of *The Payne* as a single-star spectral model $f_{\lambda, \text{single}}$.

APPENDIX B: SPECTRAL FITTING EXAMPLES

B1 Good fits

In Figure B1 we show the best fit single star and binary models for several SB2s, confirmed by changes in spectral lines over several epochs. We zoom into the wavelength range around the magnesium triplet and $H\alpha$ and in a 70 Å interval in the red arm, where many double lines are clearly visible. In the top panel we show best fit of the twin binary spectrum of J115307.93+353528.2 (denoted as “twins” in Fig. 2) taken at maximal $|\Delta \text{RV}| = 40 \text{ km s}^{-1}$, however despite double-lines are not visible, this star is selected as binary by our method. Middle panel show an example of case (ii) of SB2 fitting by the single star model, not useful for SB2 identification, however the binary model fits the spectrum well. This binary system J064726.39+223431.7 denoted as “fast” in Fig. 2. In the bottom panel we show the best fit of the binary spectrum of system J005425.62+081141.3 (denoted as “faster” in Fig. 2) of two fast rotators taken at significant $|\Delta \text{RV}|$. We will study these SB2s in Kovalev et al. (in prep.).

Fig. B2 shows a spectrum with three spectral components (SB3 J040541.37+575341.0), where the primary component of the binary model broadens to cover two out of three components. In Kovalev & Straumit (2022) we showed how such a spectrum can be disentangled.

In Fig. B3 we show the best fit single star and binary models for two SB2s, which are reported as SB1 (J085125.30+1202564) and single star (J034300.73+330448.2) in El-Badry et al. (2018). Double lines are clearly seen in the spectra, however they still can be chance alignments or the LAMOST-MRS was lucky to observe them at optimal $|\Delta \text{RV}|$.

B1.1 non-stacked spectra

In Fig. B4 we show the best fits for the non-stacked and the stacked spectra of the close binary J053818.60-091754.4. We successfully fit five individual 20 min exposures with lower $S/N_{\text{blue,red}} \sim 30, 60$ (stacked spectrum has $S/N_{\text{blue,red}} \sim 82, 143$). We find that RV rapidly changes and $V \sin i_{1,2}$ are slightly smaller ($\sim 3 - 5 \text{ km s}^{-1}$) than for the stacked spectrum. Similarly to Kovalev & Straumit (2022) we fit a circular orbit with period $P = 1.88$ days, mass ratio $q_{\text{dyn}} = 0.89$ and systemic velocity $\gamma = -13.14 \text{ km s}^{-1}$, although orbit coverage is very poor.

⁵ We used $[\text{Fe}/\text{H}]$ as a proxy of overall metallicity, abundances for all elements are scaled with Fe.

Table B1. Spectra with a problem in the wavelength calibration. Full table is available as supplementary material.

star	RV ₀ km s ⁻¹	RV ₂ km s ⁻¹	RV ₁ km s ⁻¹	MJD d
J010308.47+053110.8	232.6	-2.3	328.4	58790.635
J010355.51+052339.3	230.7	26.4	356.1	58790.635
..

B1.2 not detected SB2s

In Fig. B5 we show the best fit single star and binary models for J065032.45+231030.2 - a very interesting SB2 system of two component with $\Delta T_{\text{eff}} \sim 3000$ K, denoted as “gig” in Fig. 2. It is not selected by our criteria due to a fast rotating secondary $V \sin i = 68 \text{ km s}^{-1}$, however it can be selected based on high $f_{\text{imp}} > 0.3$ even for a spectrum with $|\Delta \text{RV}| \sim 0 \text{ km s}^{-1}$. We will study this SB2 in detail in Kovalev et al. (in prep.)

In Fig. B6 we show two SB2 systems not selected by our method. The spectrum of J055923.95+303104.2 shown in the top panel is a case (ii), where single star model fits only narrow lines of the secondary. The middle panel shows the same star without narrow lines of the secondary and the binary model consists two hot, fast rotators which is probably wrong, as their $T_{\text{eff},1,2}$ lie at edge of the model grid. The bottom panel shows the spectrum of the SB2 system J065001.65+222127.7 of two very fast rotators with insufficient $|\Delta \text{RV}|$. We will study these SB2s in detail in Kovalev et al. (in prep.)

B2 Bad fits

In Fig. B7 we show how our model desperately attempts to fit a very hot star J203746.56+421949.2 (top panel) and a very cool star J030635.12+545721.5 (bottom panel). For a hot star with emission at the $H\alpha$ core, our binary model fits “fake” system with $|\Delta \text{RV}| \sim 350 \text{ km s}^{-1}$ and good f_{imp} . For the spectrum of a cool star with clearly visible molecular bands, both models failed, but the secondary component in the binary model was able to estimate RV correctly.

B3 Bad wavelength calibration

We identify 213 spectra, where the blue and red spectral arms have nearly constant $|\Delta \text{RV}| > 180 \text{ km s}^{-1}$, after visual inspection of fits. All these spectra were observed in several particular fields and nights, thus we assume that the wavelength calibration was bad for certain fibers of the spectrograph. We list such spectra in Table B1. Examples of such spectra of the SB2 (top panel) and single star (bottom panel) are shown in Fig. B8. You can see that for a single star J093106.97+473831.4 the single star model completely failed, but the binary model was able to fit RV from the red arm by primary component and RV from the blue arm by the secondary component. For the SB2 star J121440.44+482728.0 even the binary model failed, but showed a result similar to the single star model fits on normal SB2 spectra: both components are broadened.

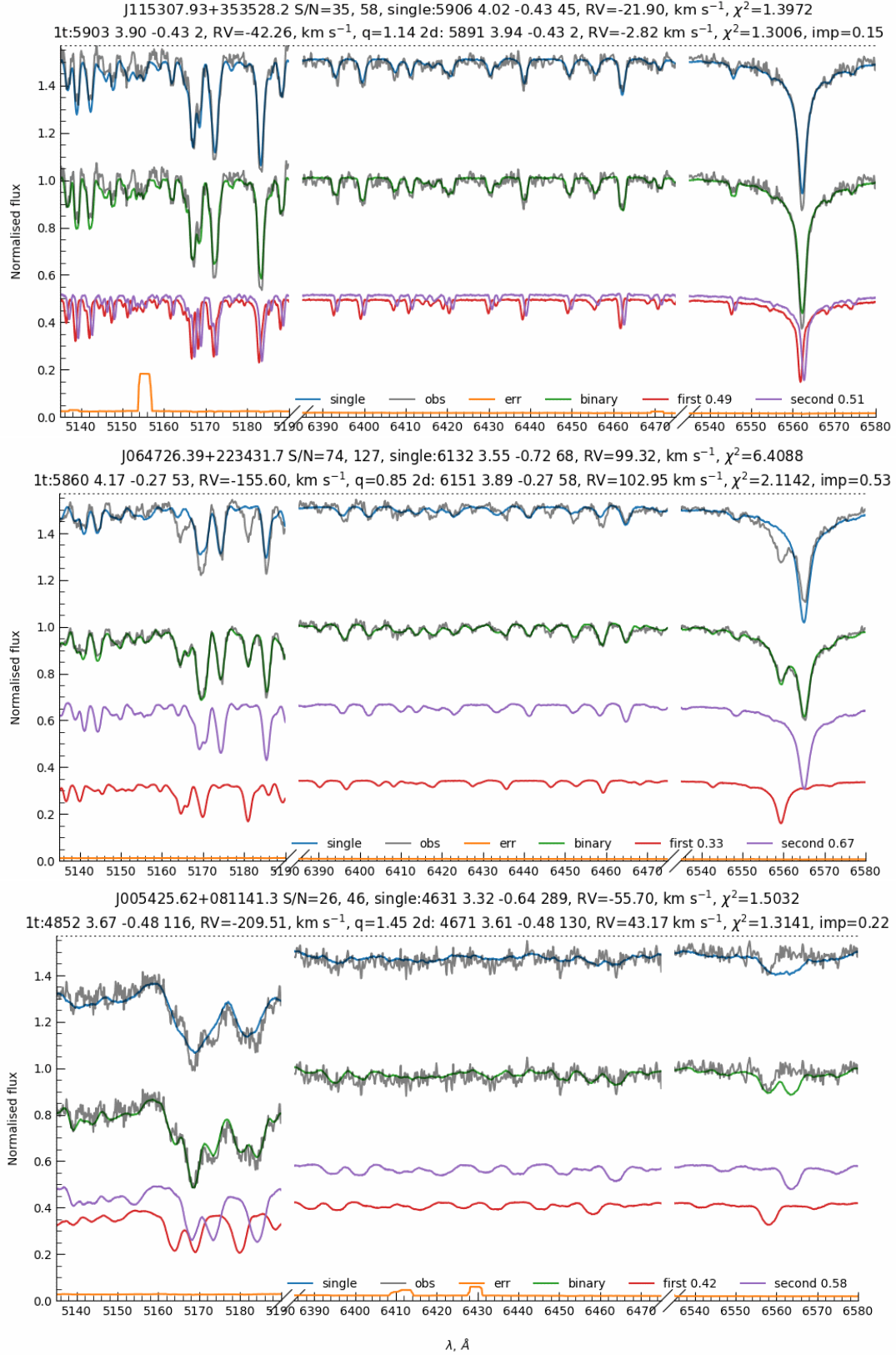


Figure B1. Examples of the spectrum fitting by binary spectral model (green line) and by single star model (blue line) (with offset 0.5). $V \sin i_{1,2}$ are increasing from the top to bottom panel. Observed spectrum and its error are shown as a gray and orange lines respectively. Primary (magenta line) and secondary (red line) components are labeled as "second" and "first" with contribution to total light at $\lambda = 5000$ Å. Spectral parameters (T_{eff} , $\log(g)$, $[\text{Fe}/\text{H}]$, $V \sin i$) from single star model fit and binary model fit are shown in the titles.

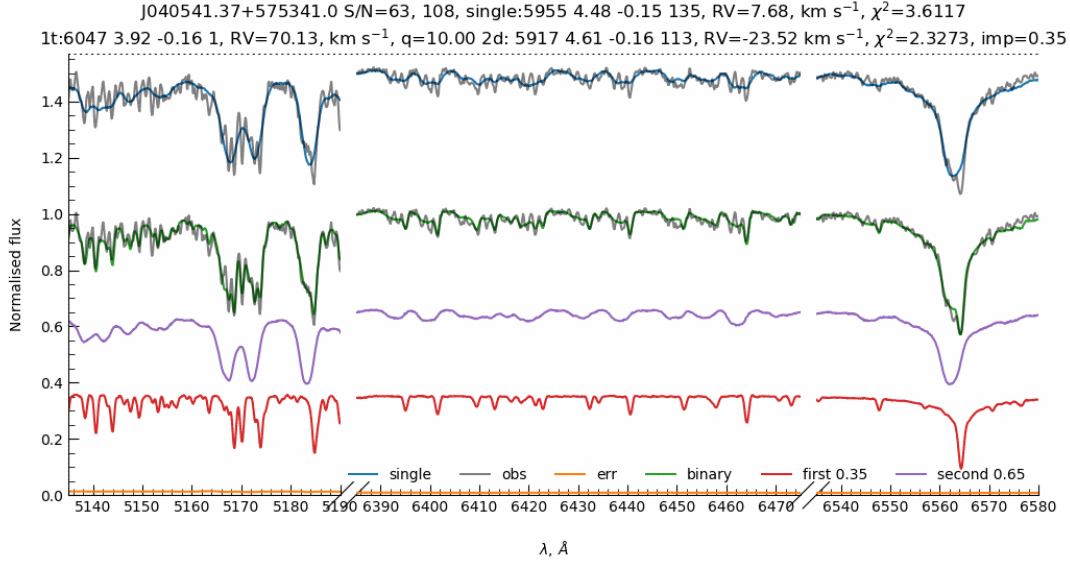


Figure B2. Same as Fig.B1 but for an SB3 candidate.

Table C1. Catalogue of SB2 candidates in LAMOST-MRS. Full table is available as supplementary material.

LAMOST designation	Gaia eDR3 source_id
J000024.99+340651.5	2875121652781859200
J000151.03+340757.3	2875206688837760640
J000223.56+340644.8	2875159070536814464
..	..

APPENDIX C: CATALOGUE OF SB2 CANDIDATES IN LAMOST-MRS

Table C1 lists all 2460 SB2 candidates. We note that LAMOST designation can slightly vary between data releases, therefore please use Gaia eDR3 source_id from Gaia Collaboration et al. (2021).

APPENDIX D: NEW SELECTION IN M 11

The new SB2 candidate is 18504350-0613598 shown on the top panel of Fig.D1. The very high mass ratio $q = 9.4$ and small $\log(g)_2 = 3.41$ dex are not realistic, probably the binary model converges to such parameters to make better fit of the light ratio. SB2 candidate 18510223-0614547 from Merle et al. (2017); Kovalev & Straumit (2022) shows clear composite spectrum (bottom panel of Fig.D1), although it is not selected due to $|RV_1 - RV_0| < 5 \text{ km s}^{-1}$ (case (ii)). All other six SB2 and one SB3 candidate from Kovalev & Straumit (2022) with $V \sin i_1 + V \sin i_2 + 5 < V \sin i_0$ are selected. Table D1 lists stellar parameters derived in Kovalev & Straumit (2022) for all 265 spectra in M 11. Plots with all 265 spectral fits will be available online <https://doi.org/10.5281/zenodo.7037605>⁶.

Table D1. Stellar parameters for all 265 M 11 stars, analysed in Kovalev & Straumit (2022). Full table in machine-readable form is available as supplementary material.

parameter	unit
CNAME	HHMMSSs+DDMMSSs
MJD	day
χ^2_{single}	
χ^2_{binary}	
f_{imp}	
α (J2000)	degree
δ (J2000)	degree
S/N	pix^{-1}
RV_0	km s^{-1}
RV_2	km s^{-1}
RV_1	km s^{-1}
q	
$\text{frac} = k/(1+k)$	
$T_{\text{eff}0}$	K
$\log(g)_0$	dex
$[\text{Fe}/\text{H}]_0$	dex
$V \sin i_0$	km s^{-1}
$T_{\text{eff}2}$	K
$\log(g)_2$	dex
$[\text{Fe}/\text{H}]_{1,2}$	dex
$V \sin i_2$	km s^{-1}
$T_{\text{eff}1}$	K
$\log(g)_1$	dex
$V \sin i_1$	km s^{-1}
Gaia eDR3 source_id	

This paper has been typeset from a \LaTeX file prepared by the author.

⁶ also available at <https://nlte.mpia.de/upload/kovalev/>

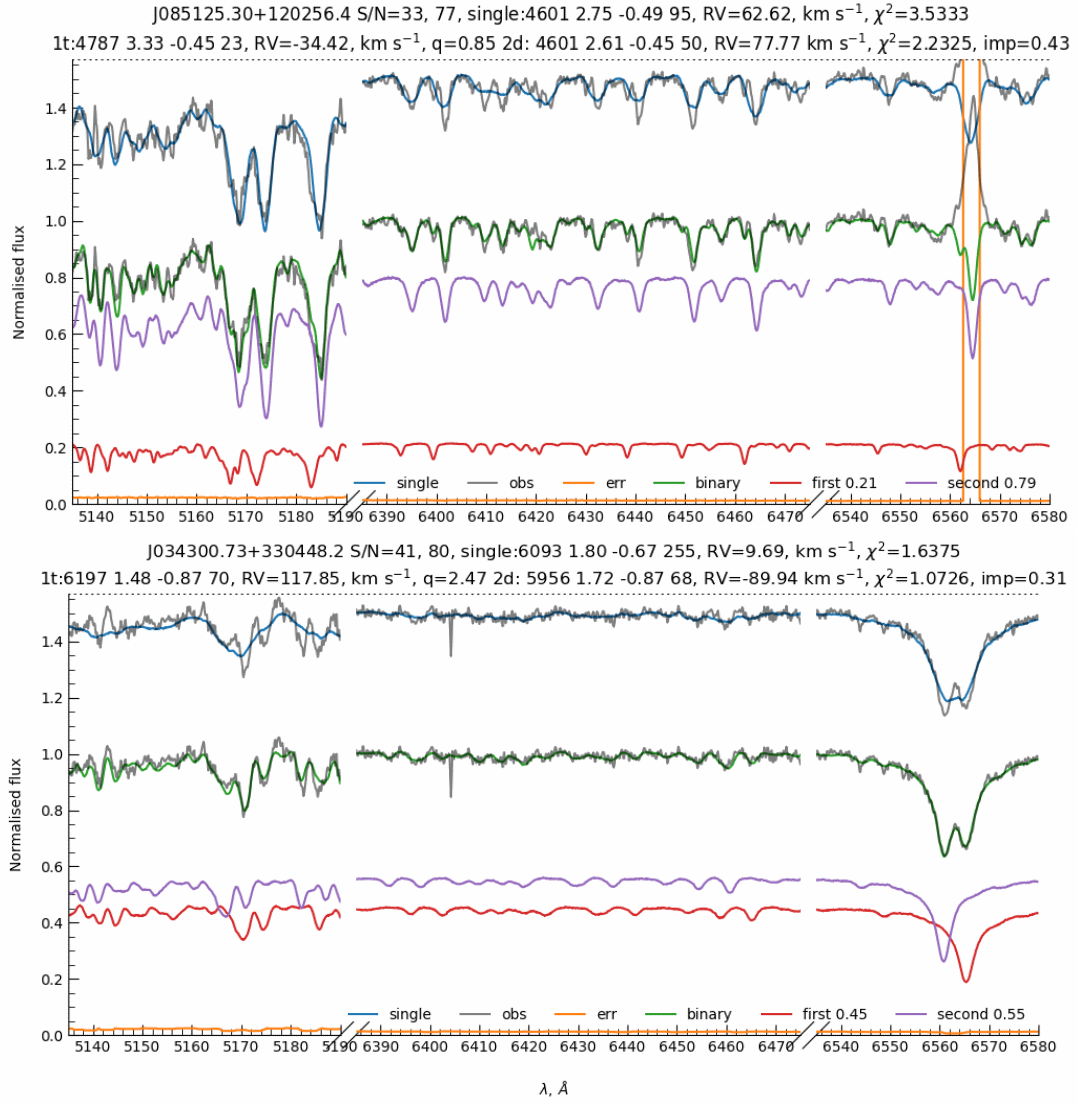


Figure B3. Same as Fig.B1 but for SB2s with matches in SB1 (top panel) and a single star (bottom panel) tables from El-Badry et al. (2018)

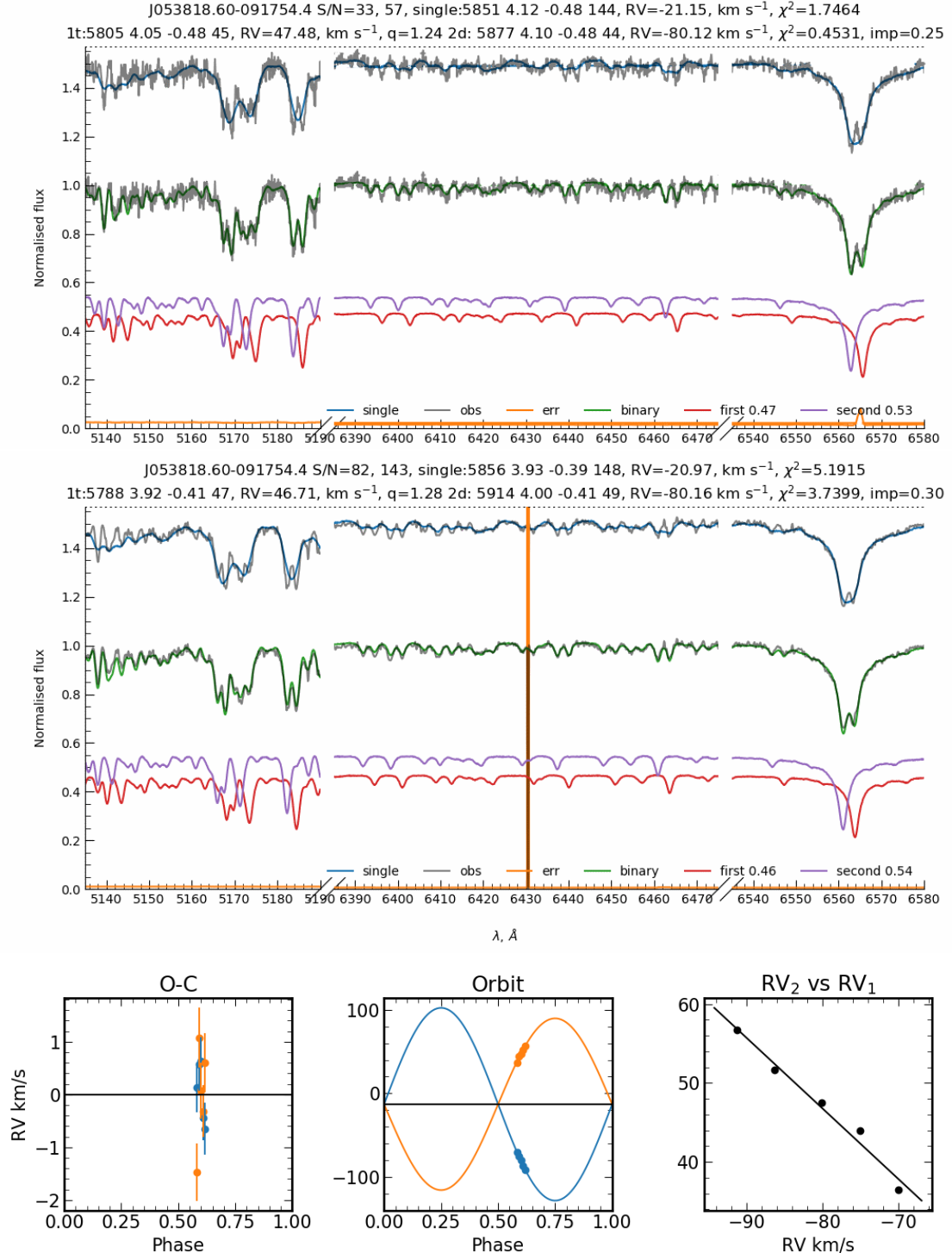


Figure B4. Same as Fig.B1 for non-stacked (top panel), stacked spectrum (middle panel) of close SB2. In the bottom panels we show a circular orbit fitting with the phase-folded RV curve in the middle, the fit residuals on the left and the Wilson plot on the right.

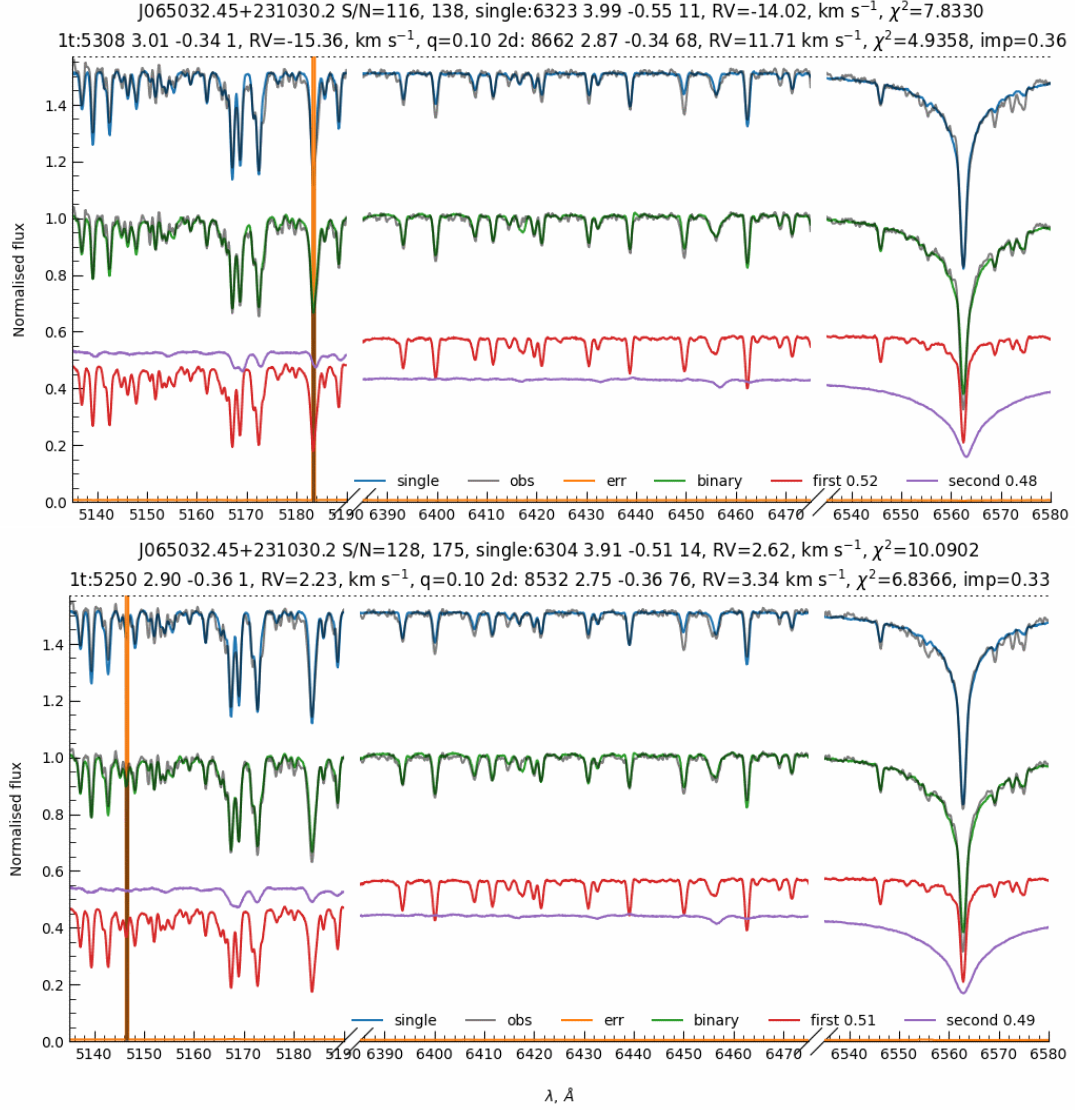


Figure B5. Same as Fig.B1 but for two spectra of SB2 system with two very different components with $\Delta T_{\text{eff}} \sim 3000 \text{ K}$. Top panel shows the spectrum with $|\Delta RV| = 27 \text{ km s}^{-1}$, and bottom panel shows the spectrum with $|\Delta RV| \sim 0 \text{ km s}^{-1}$.

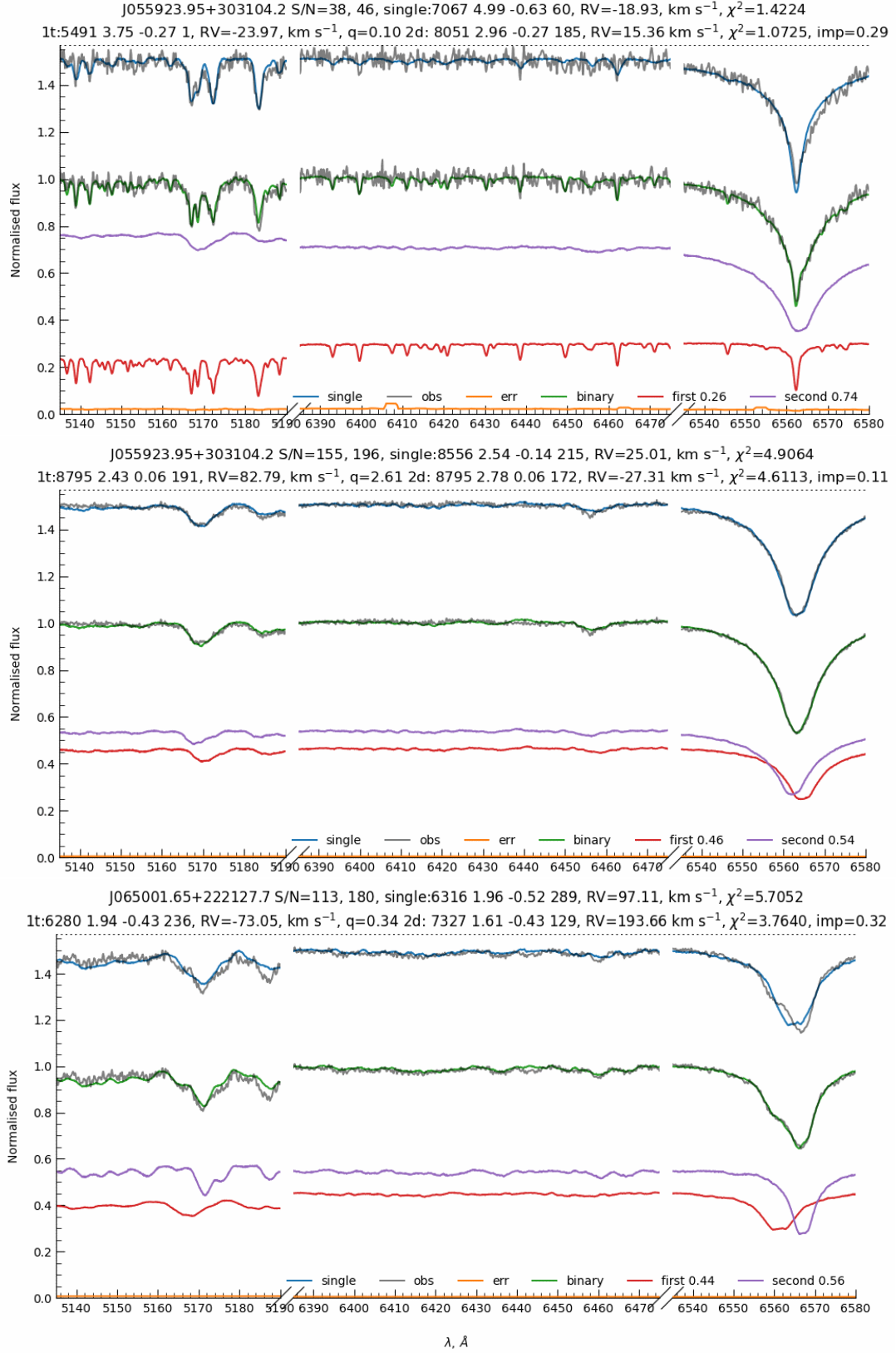


Figure B6. Same as Fig.B1 but for two SB2 systems not selected by our method. Top panel shows a spectrum, possibly taken during partial eclipse, where single star model ignores the primary component, but fits only narrow lines of the secondary. Middle panel shows the spectrum of the same star, but without narrow lines. The bottom panel shows the spectrum of an SB2 system of two very fast rotators with insufficient $|\Delta \text{RV}|$.

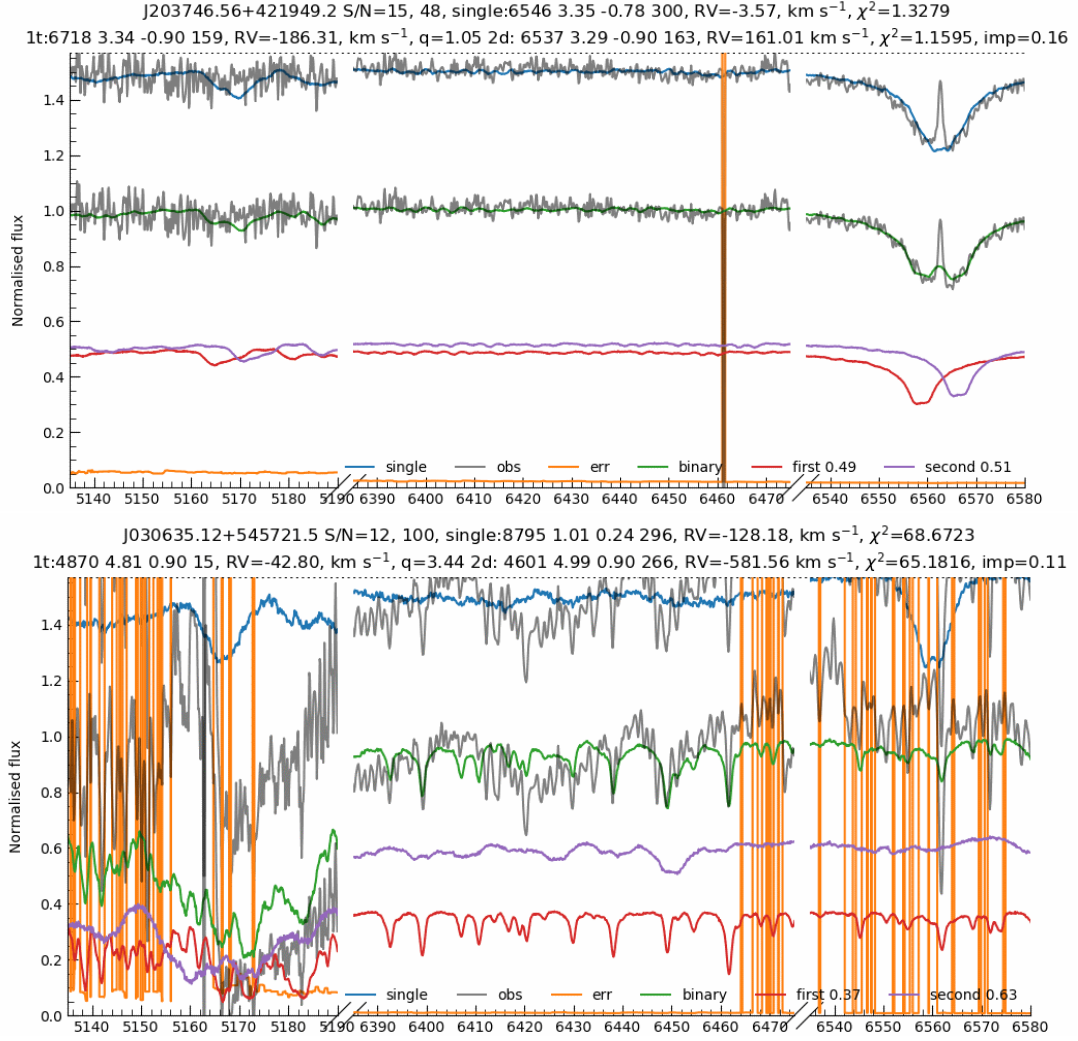


Figure B7. Same as Fig.B1 but for poor fit of a very hot star J203746.56+421949.2 (top panel) and a very cool star J030635.12+545721.5 (bottom panel)

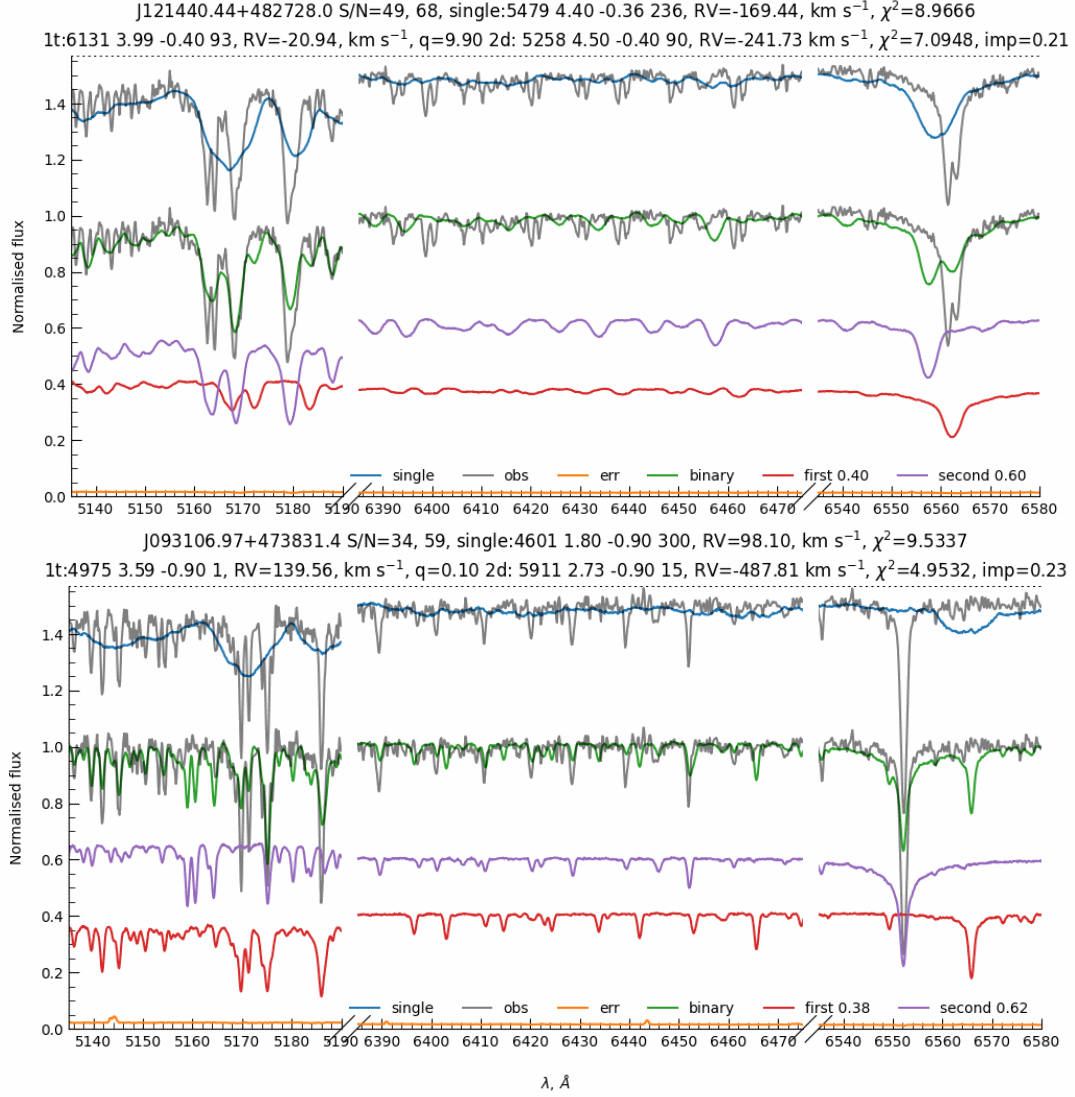
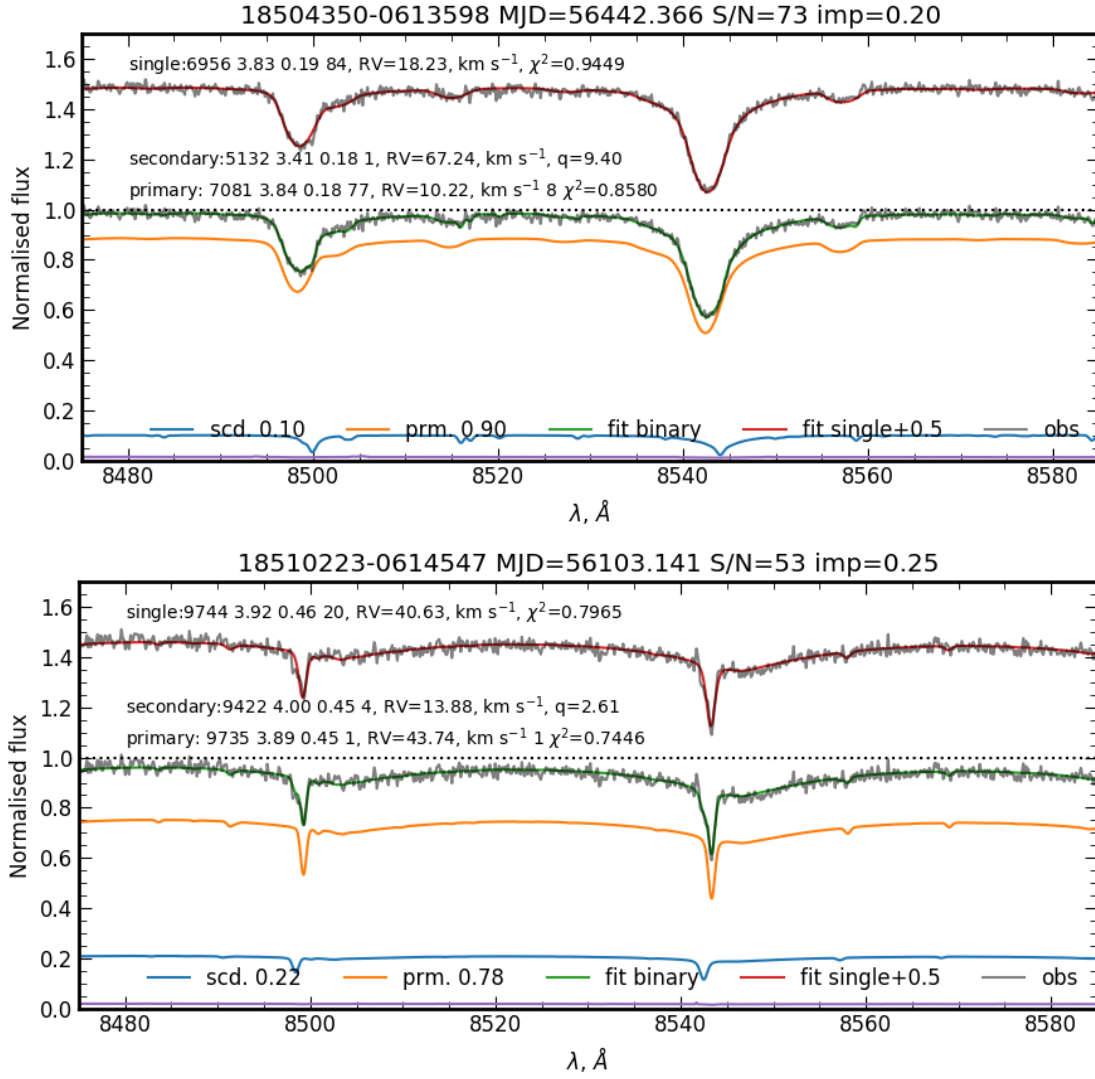


Figure B8. Same as Fig. B1 but for spectra with bad wavelength calibration. Top panel is a SB2 candidate J121440.44+482728.0 and bottom panel is a single star J093106.97+473831.4.

**Figure D1.** New (top panel) and not selected (bottom panel) SB2 candidates in M 11.